

A COMPARATIVE STUDY OF SUPERDEFORMATION IN THE $A \approx 150$ AND $A \approx 60$ NUCLEI

T.R. RAJASEKARAN, G. KANTHIMATHI

Department of Physics, Manonmaniam Sundaranar University
Tirunelveli — 627 012, India

(Received January 7, 2008)

Superdeformed (SD) bands have been identified in both the $A \approx 150$ and $A \approx 60$ regions using the statistical theory and the configuration dependent cranked Nilsson–Strutinsky (CNS) calculations. A good understanding of SD bands in different mass regions have been obtained using these models and the general features of SD bands in these mass regions are studied. Total energy surfaces (TES) have also been generated for these nuclei with in the CNS formalism to study the shape transition and oblate — prolate coexistence in detail.

PACS numbers: 21.10.Ma, 24.60.-k, 27.70.+q, 25.75.Gz

1. Introduction

To date many regions of SD nuclei have been established throughout the nuclear chart. By studying several properties of SD nuclei, the underlying shell structure of observed mass region, the high neutron scheme, some hints about specific orbital around the Fermi surface could be well understood. The existence of nuclei with such extreme deformations are explained by the occurrence of pronounced quantal level benchings ‘shells’ and consequently large shell gaps which compensate for the increased deformation energy.

The most interesting nuclear region is the one with $A \approx 150$ and $A \approx 60$ regions where a large variety of rotational structures such as smooth terminating bands, highly deformed and SD rotational bands are expected to be observed upto very high rotational frequencies on the same nucleus [1]. Particular interests are in shape transition and oblate — prolate coexistence of $N = Z$ nuclei. The limited number of particles in this nuclear region and their proximity to the $N = Z$ line make superdeformation in this mass

region of greater interest. In the present article, SD bands in ^{154}Er and ^{60}Zn are presented. In addition, the general features of SD bands in these mass regions are outlined.

Our theoretical tools are the statistical theory for hot rotating nuclei (STHRN) and the configuration dependent cranked Nilsson–Strutinsky (CNS) approach. We tried to have a better understanding of the underlying mechanism of shape evolution using these two models. In this present work, we have calculated the kinematical and dynamical moment of inertia ($j^{(1)}$ and $j^{(2)}$) of SD bands in the entire mass region using the STHRN. It provides a simple but still realistic frame to calculate moment of inertia. We emphasize particularly on $j^{(2)}$ which reflects the changes in the rotating self consistent mean field due to an internucleon interaction. We have also generated TES using the CNS formalism for all these nuclei to explore the shape transition and oblate-prolate coexistence in detail.

2. Superdeformation in the $A \approx 150$ and $A \approx 60$ regions

Superdeformed atomic nuclei with very elongated shapes are in addition to the fission isomers in actinide nuclei, now known to exist in several regions of nuclear chart. Nuclei with masses between 150 and 60 are well known to change rapidly their collective properties with proton and neutron numbers. Since the discovery of superdeformation in ^{152}Dy [2], an extensive effort has been taken in understanding nuclear structure of the states in the second minimum of potential energy in the $A \approx 150$ region. ^{154}Er is the first observation of a SD band in the $A \approx 150$ region with $Z > 66$. With the exception of nucleus ^{154}Er addressed here, there has been reasonable agreement between the experimentally determined properties of SD states and the theoretical predictions. Theoretically, Dudek *et al.* [3] have predicted that a SD band exists in ^{154}Er for relatively high spin $M \approx 44\text{--}45\hbar$ with $\beta = 0.63$ at shape parameter $\gamma = 0^\circ$ using the CNS method. On the other hand, Lagergren *et al.* [4] have observed the coexistence of SD structures at prolate and triaxial shapes. Their observation on ^{154}Er resolves the long standing difficulties in theoretical interpretation of SD shapes.

The nuclei in the $A \approx 60$ region show a remarkable diversity of shapes. Rapid changes in structure with particle number, angular momentum and excitation energy are observed. Previous studies of SD bands in $A \approx 60$ region have allowed systematic analysis of strongly deformed shapes and configurations in nuclei with $N \approx Z$ [5]. Recent works [6] predicted either an oblate to prolate or a prolate to oblate transition at low spins as well as the coexistence and strongly varying mixing of oblate and prolate deformed configurations at intermediate and high spins.

3. Formalism

3.1. Statistical theory for hot rotating nuclei

In heavy-ion collision, the foremost motivation behind the investigation on high spin states is to evaluate the probability for phenomena such as fusion, fission and quasi-fission. Statistical approach is the most prominent one to describe the average behaviour of the compound nucleus. Bethe and Ericson [7] utilized statistical models to understand the nuclear properties. Further Moretto [8] extended the model by means of the single particle levels of deformed nuclei in which a Lagrangian multiplier projects out different angular momentum states of the system from the grand partition function. The development of STHR_N by us has resulted in successful application of this theory to high spin nuclei [9].

It can be easily shown as in Refs. [10] and [11] that the n -th derivate of $\ln Z(\alpha, \beta, \omega)$ where $Z(\alpha, \beta, \omega)$ is the grand partition function,

$$\ln Z(\alpha, \beta, \omega) = \sum_k \ln [1 + \exp[-\beta(\epsilon_k(\omega) + \alpha)]] , \quad (1)$$

with respect to the Lagrangian multipliers (α, β, ω) which conserve the particle number and energy yields the corresponding n -th moments of the observable energy E and particle number N . The relevant equations [12] in terms of single particle energies $\epsilon_k(\omega)$ and spins m_k (projection along the symmetry axis) are,

$$\langle N \rangle = \sum_k [1 + \exp(\beta\epsilon_k^N(\omega) - \alpha_N)]^{-1} = \sum_k n_k^N , \quad (2)$$

$$\langle Z \rangle = \sum_k [1 + \exp(\beta\epsilon_k^Z(\omega) - \alpha_Z)]^{-1} = \sum_k n_k^Z , \quad (3)$$

$$\langle E(\omega, T) \rangle = \sum_k n_k^N \epsilon_k^N(\omega) + \sum_k n_k^Z \epsilon_k^Z(\omega) , \quad (4)$$

$$\langle M \rangle = \sum_k n_k^N m_k^N(\omega) + \sum_k n_k^Z m_k^Z(\omega) . \quad (5)$$

In the above equations, the superfix N and Z refer to the single particle values corresponding to neutrons and protons. The Lagrangian multipliers α_N and α_Z are fixed by equations (2–5). The simultaneous non-linear equations (2), (3) and (5) are solved to determine α_N and α_Z for each value of the rotational frequency ω and $\beta(= 1/T)$, the reciprocal of the temperature T . The excitation energy of the system is given by

$$E^*(\omega, T) = E(\omega, T) - \left\{ \sum_{k=1}^N \epsilon_k^N(0) + \sum_{k=1}^Z \epsilon_k^Z(0) \right\} , \quad (6)$$

where the sum of the second and third terms yield the ground state energies of neutrons and protons. The free energy expression is given by

$$F(\omega, T) = E(\omega, T) - TS, \quad (7)$$

where S is the entropy of the system.

$$S = \sum_k [n_i^N \ln n_i^N + (1 - n_i^N) \ln (1 - n_i^N)] \\ + \sum_k [n_i^Z \ln n_i^Z + (1 - n_i^Z) \ln (1 - n_i^Z)]. \quad (8)$$

In this method only the z component M of the total angular momentum I is considered. As mentioned by Moretto [8] the laboratory fixed z axis can be made to coincide with the body fixed z' axis and it is possible to identify and substitute M for the total angular momentum I . Within the limit of quantum mechanics, the z component of the total angular momentum is $M \rightarrow \sqrt{I(I+1)} = I + 1/2$ where I is the total angular momentum of the system.

The nuclear level density at an excitation energy $E^*(\omega, T)$ is given by [13]

$$\rho(E^*) = \frac{(\hbar^2/2\theta)^{3/2}(2I+1)\sqrt{a} \exp(2\sqrt{aE^*(\omega, T)})}{12(E^*(\omega, T) + T)^2}, \quad (9)$$

where θ is the rigid body moment of inertia and a is the single particle level density parameter. The kinematical and dynamical moment of inertia $j^{(2)}$ are given by [14]

$$j^{(1)} = \hbar^2 I \left(\frac{\partial E_{\text{rot}}}{\partial I} \right)^{-1}, \quad (10)$$

$$j^{(2)} = \hbar^2 \left(\frac{\partial^2 E_{\text{rot}}}{\partial^2 I} \right)^{-1}, \quad (11)$$

where the rotational energy E_{rot} for given ω and T is

$$E_{\text{rot}} = E(\omega, T) - E(0, T). \quad (12)$$

The single particle energies $\epsilon_k(\omega)$ and spin projections m_k are generated by diagonalizing the Hamiltonian in the oscillator basis.

$$H^\omega = H^O - \omega j, \quad (13)$$

where ω is the rotational frequency and H^O is the triaxial Nilsson-Hamiltonian for a single particle in the non-rotating system and is given by

$$H^O = \frac{p^2}{2m} + \frac{m}{2} (\omega_x^2 x^2 + \omega_y^2 y^2 + \omega_z^2 z^2) + Cl.s + D (l^2 - 2 \langle l^2 \rangle). \quad (14)$$

The oscillator frequencies are

$$\omega_x = \omega_0 \left[1 + \frac{1}{3}\varepsilon \cos \gamma + \frac{1}{\sqrt{3}}\varepsilon \sin \gamma \right], \quad (15)$$

$$\omega_y = \omega_0 \left[1 + \frac{1}{3}\varepsilon \cos \gamma - \frac{1}{\sqrt{3}}\varepsilon \sin \gamma \right], \quad (16)$$

$$\omega_z = \omega_0 \left[1 - \frac{2}{3}\varepsilon \cos \gamma \right], \quad (17)$$

where the parameter ε corresponds to the elongation or flattening of the potential while γ describes its non-axiality.

The Lagrangian multiplier γ and the collective frequency of rotation ω of the system should be equal to one another as long as the single particle spin projections along the symmetry axis are good quantum numbers [12]. For axially symmetric shapes of the nuclei, the single particle spin projections m_z are good quantum numbers while for triaxial deformations the single particle spin projections m_z are not good quantum numbers as the matrix elements for triaxially deformed system connects states of different m_z . To overcome this problem one can use cranked Nilsson–Strutinsky model which has important achievements like the prediction of SD high spin states and terminating bands [15].

Calculations are carried out for the deformation parameter $\varepsilon = 0.0\text{--}0.7$ in steps of 0.1 and for shape parameter $\gamma = -180^\circ$ (non-collective oblate shape rotating about the symmetry axis) to $\gamma = -120^\circ$ (collective prolate shape rotating about an axis perpendicular to the symmetry axis).

3.2. The cranked Nilsson–Strutinsky model

The main idea of the Nilsson–Strutinsky approach [16] is to split the total energy of the nucleus into two parts, an usual part parameterized by a macroscopic expression, and a fluctuating part obtained from the variation of the level density around the Fermi surface. The microscopic part comprises the Strutinsky shell correction and the pairing energy. Rotation is introduced in the cranking approximation, corresponding to rotation around one principal axis. The Hamiltonian can be expressed as

$$H^\omega = H^O - \omega j_x = H_{\text{HO}}(\varepsilon, \gamma) + 2\hbar\omega_o\rho^2\sqrt{\frac{4\pi}{9}}\varepsilon_4V_4(\gamma) + V' - \omega j_x, \quad (18)$$

where $H_{\text{HO}}(\varepsilon, \gamma)$ is the anisotropic harmonic oscillator potential.

$$H_{\text{HO}}(\varepsilon, \gamma) = \frac{p^2}{2m} + \frac{1}{2}m\{\omega_x^2x^2 + \omega_y^2y^2 + \omega_z^2z^2\}. \quad (19)$$

Here ω_x , ω_y and ω_z are the oscillator frequencies expressed in terms of the quadrupole deformation parameters with signs chosen according to the Lund convention [17]

$$\omega_j = \omega_0(\varepsilon, \gamma) \left[1 - \frac{2}{3} \varepsilon \cos \left(\gamma + \frac{2\pi\nu_j}{3} \right) \right], \quad j \in \{x, y, z\}, \quad (20)$$

with $\nu_x = 1$, $\nu_y = -1$ and $\nu_z = 0$. The calculations are carried out in the stretched coordinate system. The hexadecapole potential is chosen to attain a smooth variation in the γ plane so that axial symmetry is not broken for $\gamma = -120^\circ, -60^\circ, 0^\circ$ and 60° . The parameters κ and μ might be given the same values for each shell instead they could be made dependent on the main oscillator quantum number $N = N_t$. The eigenvalues e_i^ω and the eigenvectors χ_i^ω are obtained by diagonalizing the Hamiltonian.

Now, the single particle energies and the single particle spin contributions m_i are obtained in the laboratory system as

$$e_i = \langle \chi_i^\omega | H^0 | \chi_i^\omega \rangle, \quad (21)$$

$$m_i = \langle \chi_i^\omega | j_x | \chi_i^\omega \rangle, \quad (22)$$

where H^0 is the static single-particle Hamiltonian.

The total quantities can be expressed as

$$E_{\text{sp}} = \sum_{\text{Occ}} e_i = \sum_{\text{Occ}} e_i^\omega + \hbar\omega \sum_{\text{Occ}} m_i, \quad (23)$$

$$I = \sum_{\text{Occ}} m_i, \quad (24)$$

with the summation over the occupied orbitals in a specific configuration of the nucleus. The shell energy is now evaluated from

$$E_{\text{shell}}(I) = E_{\text{sp}}(I) - \langle E_{\text{sp}}(I) \rangle, \quad (25)$$

where $\langle E_{\text{sp}}(I) \rangle$ is the smoothed single particle sum.

An important correction is the pairing energy which should decrease with increasing spin and becomes insignificant at very high spins. To obtain an ($I = 0$) average pairing gap Δ , which varies as $A^{-\frac{1}{2}}$, the pairing strength G is chosen as,

$$G_{Z,N} = \frac{1}{A} \left[g_0 \pm g_1 \frac{N - Z}{A} \right], \quad (26)$$

with $g_1/g_0 \approx 1/3$. Also, the number of orbitals incorporated in the pairing calculation should differ as \sqrt{Z} and \sqrt{N} for protons and neutrons. The total nuclear energy is now obtained by substituting the smoothed single particle sum with the rotating liquid drop energy including the pairing correction.

$$E_{\text{tot}}(\bar{\varepsilon}, I) = E_{\text{shell}}(\bar{\varepsilon}, I) + E_{\text{RLD}}(\bar{\varepsilon}, I) + E_{\text{pair}}(\bar{\varepsilon}, I), \quad (27)$$

where $\bar{\varepsilon} = (\varepsilon, \gamma, \varepsilon_4)$. The shell and pairing energies are calculated separately for protons and neutrons at $I = 0$, while the renormalization of the moment of inertia introduces a coupling when evaluating E_{shell} for $I > 0$. In the present work, E_{pair} is included only for $I = 0$.

4. Results and discussions

The results of the nuclear level density (NLD) for ^{154}Er as a function of deformation and excitation energy for selected spins is depicted in Fig. 1. It is very important to remember that the NLD not only determines the deformation probability distribution but also the population probability. The

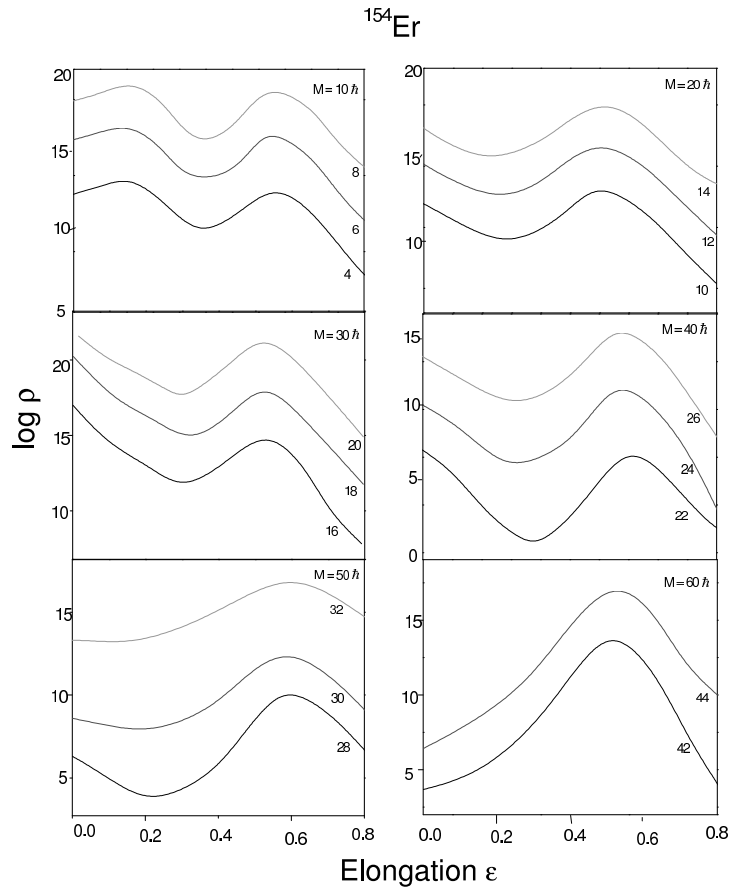


Fig. 1. Nuclear level density *versus* temperature for different angular momentum for ^{154}Er . The numbers on the curve refer to the excitation energy in MeV.

domination of level density at the normal deformed (ND) range over the SD range is observed to be very strong in the case of spin $M = 30\hbar$, the population of the ND states dominate while at $M = 40\hbar$ none of the configurations would be strongly discriminated against the other. In fact $M = 40\hbar$ is the cutoff spin at which the side feeding of the SD band decreases or practically disappears. At higher spin values $M = 46\hbar$ the population of the SD states is significantly favored. Similar effects are shown in Fig. 2 for ^{60}Zn . Here the cutoff spin is $M = 8\hbar$ at which the population of the SD states are significantly favored. At cutoff spin $M = 8\hbar$, the side feeding of the SD band decreases for the nucleus and for $M > 8\hbar$ the population of SD states is dominant.

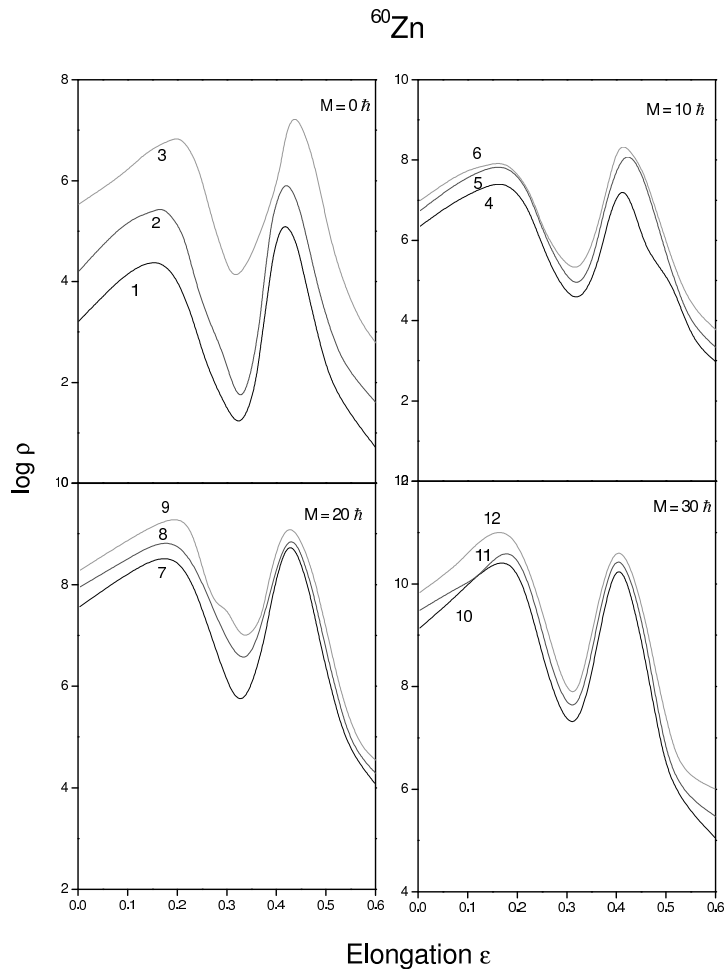


Fig. 2. Same as Fig. 1 for ^{60}Zn .

Figs. 3 and 4 show the dynamical moment of inertia obtained using equation (11) compared with the experimental data of Bernstein *et al.* [18]. In the more axially deformed SD nuclei in the $A \approx 150$ mass region, the $j^{(2)}$ have been reproduced well with some small variances. The observed $j^{(2)}$ does not involve any humps which indicate that single particle configuration of SD bands involves band crossing. The most pronounced feature in Fig. 3 is that the $j^{(2)}$ of this sort corresponds to a rapid gain in alignment (spin) which may occur following the rotation-induced alignment of a pair of particles (paired band crossing). The observed rise in $j^{(2)}$ corresponds to the alignment of two $N = 7$ quasi neutrons. It is also observed from Fig. 3 that the rapid rise of $j^{(2)}$ occurs for a small range of $\hbar\omega$. This property indicates a relatively weak interaction between the crossing orbital. A similarity of the low frequency rise in $j^{(2)}$ between the theoretical values and the experimental data is also observed from the close inspection of the Fig. 3.

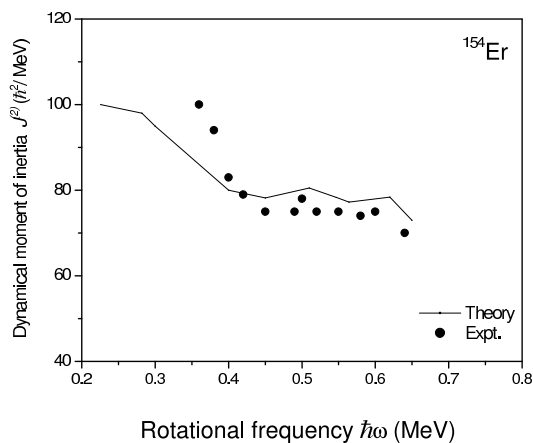


Fig. 3. Dynamical moment of inertia $j^{(2)}$ versus rotational frequency $\hbar\omega$ for ^{154}Er .

In Fig. 4 the occurrence of peak of $j^{(2)}$ at low spin is observed for ^{60}Zn . The simultaneous alignments of the $g_{9/2}$ protons and neutrons are the reason for the peak in ^{60}Zn . This interpretation is very difficult to understand in view of the absence of any alignment gain in ^{61}Zn [19]. In Ref. [19] they have offered a tentative explanation to this anomaly in terms of a change in the pairing correlation and they have concluded that the peak in the $j^{(2)}$ of ^{60}Zn is due to the crossing of the $T = 1$ and $T = 0$ bands. To support or disprove such a hypothesis, more experimental especially theoretical investigations of properties of odd and odd-odd nuclei around ^{60}Zn are needed. The present paper supports and confirms the peak of $j^{(2)}$ at low angular frequency using STHR. It is found that much lower values of $j^{(1)}$ and $j^{(2)}$ at high spin is rather a general feature of SD bands in this mass region [20].

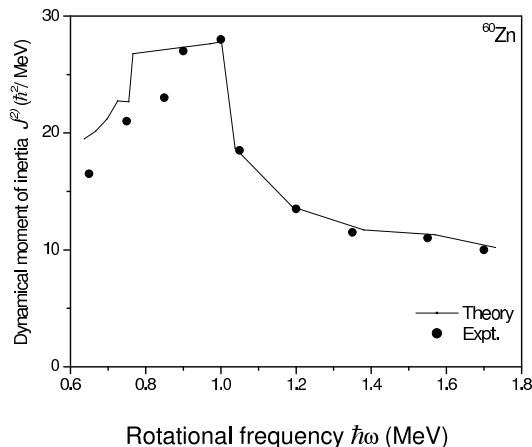


Fig. 4. Same as Fig. 3 for ^{60}Zn .

Several features of these bands are similar to those of smooth terminating bands observed in the $A \approx 110$ mass region. Such features are the smooth drop of $j^{(2)}$ with increasing rotational frequency to values much lower than $j^{(1)}$. Indeed in the $A \approx 60$ mass region, one can see the gradual transition from the smooth terminating bands in $^{62,64}\text{Zn}$ over the highly deformed band in ^{58}Cu to the SD bands in $^{60,62}\text{Zn}$. Thus a rigid rotor assumption ($j^{(1)} \approx j^{(2)}$) sometimes used in the analysis of SD bands is not valid in this mass region. The rotational sequences in the mass 60 region serve also as a contrast to those in the “traditional” regions of superdeformation at mass 80 because of the occurrence of a so called smooth band termination. Such an effect is expected in these relatively light nuclei, which have a smaller number of valence particles than the heavier nuclei and this exhaust the angular momentum content of their single particle configurations faster than the heavier nuclei.

Figs. 5 and 6 represent the rotational frequencies generated at different angular momentum and different temperatures for ^{154}Er and ^{60}Zn , respectively. It is obvious from the figures that higher cranking frequency values are required to generate particular angular momentum. However this kind of behavior is observed upto angular momentum $M = 46\hbar$ for ^{154}Er and $M = 8\hbar$ for ^{60}Zn where the shape transition occurs. The fluctuations in Fig. 5 for ^{154}Er and Fig. 6 for ^{60}Zn indicate the shape transition with respect to angular momentum for $\varepsilon = 0.0-0.7$, respectively.

The hodograph with the deepest energy minimum of ^{154}Er and ^{60}Zn as a function of angular momentum and deformation parameters ε and γ calculated for temperatures $T = 0.2$ MeV and $T = 0.3$ MeV are depicted in Figs. 7 and 8. Fig. 7 shows that the nucleus is oblate with $\varepsilon = 0.1$

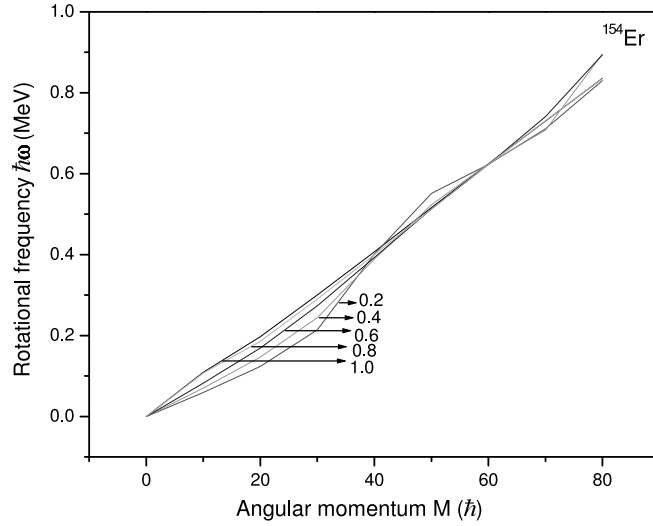


Fig. 5. Rotational frequency $\hbar\omega$ as a function of angular momentum M for different temperatures in the case of ^{154}Er . The numbers on the curve refer to the temperature T in units of MeV.

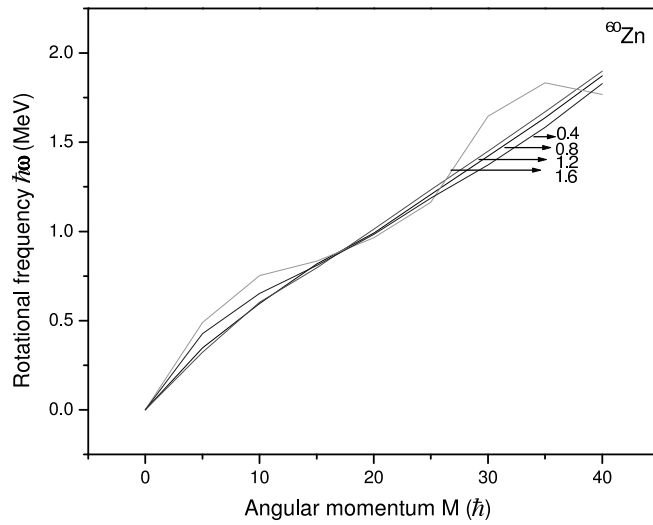


Fig. 6. Same as Fig. 5 for ^{60}Zn .

and $\gamma = -180^\circ$ for angular momentum $0-45\hbar$ and prolate for $46-60\hbar$ with $\varepsilon = 0.5$ and $\gamma = -120^\circ$. From Fig. 8 it is observed that the nucleus is prolate with $\varepsilon = 0.1$ and $\gamma = -120^\circ$ for angular momentum $0-7\hbar$ and it retains the prolate shape with $\varepsilon = 0.5$ from $M = 8-30\hbar$.

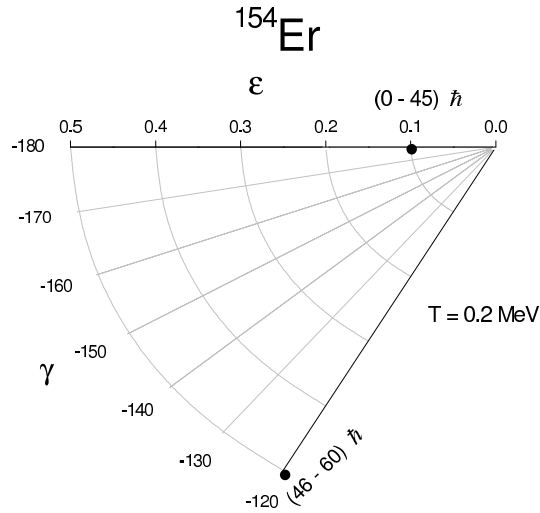


Fig. 7. Shape evolution of ^{154}Er as a function of angular momentum M using total energy surfaces at temperature $T = 0.2$ MeV.

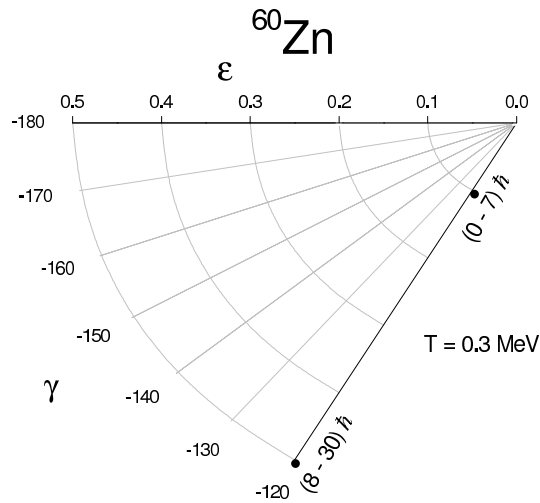


Fig. 8. Same as Fig. 7 for ^{60}Zn at $T = 0.3$ MeV.

In our calculations with shape fluctuations the key factor is the free energy $F(\epsilon, \gamma)$ because its exponential part provides the weight of each point (ϵ, γ) in the evaluation of expectation energy values. The total energy surfaces are also computed at temperature $T = 0.2$ MeV for angular momentum $0-60\hbar$. The results clearly show the shape evolution of the nucleus

leading to a shape transition from oblate to prolate. From angular momentum $M=0-45\hbar$ the absolute minima correspond to an oblate ($\varepsilon = 0.1$ and $\gamma = -180^\circ$). Beyond $M = 45\hbar$ the shape is shifted to prolate superdeformed ($\varepsilon = 0.6$ and $\gamma = -120^\circ$). In addition to the minima of prolate shape a triaxial minimum is associated with the earlier minima from the angular momentum $M = 46\hbar$. This is in agreement with the triaxial and prolate SD configurations obtained for ^{154}Er [4] with rotational frequencies $\hbar\omega = 0.53$ MeV and $\hbar\omega = 0.62$ MeV, respectively. Thus from TES it is inferred that the nucleus has two minima one corresponds to a prolate SD shape and the other relates to triaxial SD shape. The configuration of the triaxial SD shape is due to the presence of intruder orbitals.

The doubly magic even nucleus ^{60}Zn is at prolate shape from spin $M = 0-30\hbar$ and the deformation parameter varies from $\varepsilon = 0.1$ to 0.5 at $M = 8\hbar$. It seems that a prolate superdeformed structure exists from $M = 8\hbar$ ($\gamma = -120^\circ$) and remains superdeformed till $M = 30\hbar$. This result is in consistent with the doubly magic SD band obtained in the $N = Z$ nucleus ^{60}Zn in Ref. [6]. These bands are understood to be multiple excitations of $\pi f_{7/2}$ and $\nu f_{7/2}$ particles in to $\pi g_{9/2}$ and $\nu g_{9/2}$ intruder orbitals near the $N = Z = 30$ SD shell gaps [21].

5. Conclusion

It is observed from the results that at finite temperature the nuclei undergo shape fluctuations around most probable configuration. The most relevant fluctuations are those related to collective degrees of freedom, *i.e.* shape parameters ε and γ and pairing gap Δ . A microscopic calculation taking into account all these degrees of freedom is not considered in this study and only the role played by shape fluctuations for the nuclei ^{154}Er and ^{60}Zn are concentrated. Further experimental study of SD bands in these mass regions as well as theoretical studies of the decay out process tailored specifically to these regions, will undoubtedly lead to a strong understanding of both superdeformation in these regions and the decay out of SD bands in general.

This work is supported by the project (No. 2003/37/27/BRNS/1988) sanctioned under the Department of Atomic Energy — the Board of Research in Nuclear Science, India.

REFERENCES

- [1] A.V. Afanasjev, G. Lalazissis, P. Ring, *Nucl. Phys.* **A634**, 395 (1998).
- [2] P.J. Twin *et al.*, *Phys. Rev. Lett.* **57**, 811 (1986).
- [3] J. Dudek, W. Nazarewicz, *Phys. Rev.* **C31**, 298 (1985).

- [4] K. Lagergren *et al.*, *Phys. Rev. Lett.* **87**, 022502 (2001).
- [5] W. Satula *et al.*, *Phys. Rev. Lett.* **86**, 4488 (2001).
- [6] K. Kaneko, M. Hasegawa, T. Mizusaki, *Phys. Rev.* **C70**, 051301(R) (2004).
- [7] H. Bethe, *Phys. Rev.* **50**, 332 (1936); T. Ericson, *Adv. Phys.* **9**, 425 (1960).
- [8] L.G. Moretto, *Nucl. Phys.* **A182**, 641 (1972).
- [9] T.R. Rajasekaran, G. Kanthimathi, *Eur. Phys. J.* **A35** (2008), in press.
- [10] M. Rajasekaran, N. Arunachalam, T.R. Rajasekaran, V. Devanathan, *Phys. Rev. Lett.* **61**, 2007 (1988).
- [11] M. Rajasekaran, T.R. Rajasekaran, N. Arunachalam, V. Devanathan, *Phys. Rev.* **C38**, 1926 (1988).
- [12] M. Rajasekaran, T.R. Rajasekaran, N. Arunachalam, *Phys. Rev.* **C37**, 307 (1988).
- [13] K. Snover, *Annu. Rev. Part. Nucl. Sci.* **36**, 545 (1986).
- [14] T.R. Rajasekaran, S. Selvaraj, S. Santhosh Kumar, *Pramana* **60**, 75 (2003).
- [15] I. Ragnarsson *et al.*, *Nucl. Phys.* **A347**, 287 (1980).
- [16] T. Bengtsson *et al.*, *Phys. Scr. T* **5**, 165 (1983).
- [17] G. Andersson *et al.*, *Nucl. Phys.* **A268**, 205 (1976).
- [18] L.A. Bernstein *et al.*, *Phys. Rev.* **C52**, R1171 (1995).
- [19] C.H. Yu *et al.*, *Phys. Rev.* **C60**, 031305 (1983).
- [20] J. Dobaczewski, J. Dudek, R. Wyss, *Phys. Rev.* **C67**, 034308 (2003).
- [21] C.E. Svensson *et al.*, *Phys. Rev. Lett.* **79**, 1233 (1997).